Electron transport properties of graphene nanoribbons with Gaussian deformation

Van-Truong Tran [1,*] Jérôme Saint-Martin,[2] and Philippe Dollfus[2]

[1]*IMPMC, Université Pierre et Marie Curie (UPMC), Sorbonne Universités, 75252 Paris Cedex 05, France*
[2]*Université Paris-Saclay, CNRS, Centre de Nanosciences et de Nanotechnologies, 91120 Palaiseau, France*

Gaussian deformation in graphene structures exhibits an interesting effect in which flower-shaped confinement states are observed in the deformed region [Carrillo-Bastos *et al.*, Phys. Rev. B **90**, 041411 (2014)]. To exploit such a deformation for various applications, tunable electronic features including a band-gap opening for semimetallic structures are expected. Besides, the effects of disorders and external excitations also need to be considered. In this work, we present a systematic study on quantum transport of graphene ribbons with Gaussian deformation. Different levels of deformation are explored to find a universal behavior of the electron transmission. Using a tight-binding model in combination with nonequilibrium Green's-functions formalism, we show that the first plateau of the transmission of semimetallic armchair ribbons is just weakly affected in the case of small Gaussian deformations. However, significant large Gaussian bumps can induce a strong drop of this plateau and a transport gap is formed. The transmission at zero energy is found to decrease exponentially with increasing the size of the Gaussian bump. Moreover, the gap of semiconducting ribbons is enlarged with large deformations. The opening or the widening of the transport gap in large deformed armchair structures is interpreted by a formation of a spatially three-zone behavior of the hopping profile. On the other hand, a transport gap is not observed in zigzag ribbons regardless of the size of Gaussian bumps. This behavior is due to the strong localization of edge states at the energy point $E = 0$. Furthermore, it unveils the opposite effect of vertical electric fields $+E_z$ and $-E_z$, stemming from the breaking of the mirror symmetry. Additionally, it is also pointed out that the electronic behavior of a Gaussian deformed ribbon including edge roughness is dominated by the characteristics of the edge-roughness effect with strong Anderson-type localized states reflected by sharp peaks in the transmission profile.

I. INTRODUCTION

Graphene has been recognized as a material for the future of electronics due to its exceptional electronic properties with the extremely high electron mobility and the form of a thin layer structure. All these intriguing features could lead to compact and efficient electronic devices [1]. However, two-dimensional (2D) graphene is a semimetallic material [2] and exhibits an almost zero band gap that limits its possible applications in electronics. Interestingly, it has been demonstrated that narrow ribbons of graphene possess a finite band gap [3,4] and promise to be suitable for different applications such as transistors [5,6] and thermoelectric generators [7–9].

To push graphene ribbons closer to real applications, further studies of more realistic structures of ribbons containing defects such as vacancies [9–12] and edge roughness [10,13–16] have been taken up. It has been shown that such defects strongly influence the natural electronic properties of ribbons. Defects lead to a suppression of the electrical conductance depending on the vacancy position [9] and the level of vacancies [11]. Besides, edge roughness may lead to strong Anderson localization in areas of edge roughness [14].

Another type of disorder has been also paid attention which is deformation. In-plane deformation in ribbon structures was

studied by Chang *et al.* in 2007 [17] and, subsequently, additional works [18–22] have been carried out by other groups to provide a more comprehensive understanding of this effect. It has been unveiled that under a uniaxial strain, the electronic properties of zigzag graphene nanoribbons (ZGNRs) are almost unchanged while the band gaps of armchair graphene nanoribbons (AGNRs) are observed to fluctuate with the applied uniaxial strain [18]. Grain boundary can also be considered as a local in-plane deformation [23,24] with a significant impact on the electronic transport properties [24].

On the other hand, the presence of out-of-plane deformation has been evidenced in many structures [25]. This kind of disorder has been examined recently on both 2D graphene [25–29] and ribbons [30–34]. It has been shown that graphene deposited on a low-quality substrate can contain out-of-plane deformations, and Gaussian deformations are frequently observed [25]. A Gaussian bump can also be generated during a scanning tunneling microscope (STM) process when the STM tip can interact with the graphene layer via van der Waals interactions [35].

The presence of deformation leads to a change in the mechanical properties of ribbons and also in the electronic ones. Recent studies have shown an interesting phenomenon in which flower-shaped confinement states are observed in centrosymmetric Gaussian deformed regions [31]. Additionally, a local sublattice breaking symmetry is found, i.e., an unequal distribution of charge density between the two nonequivalent
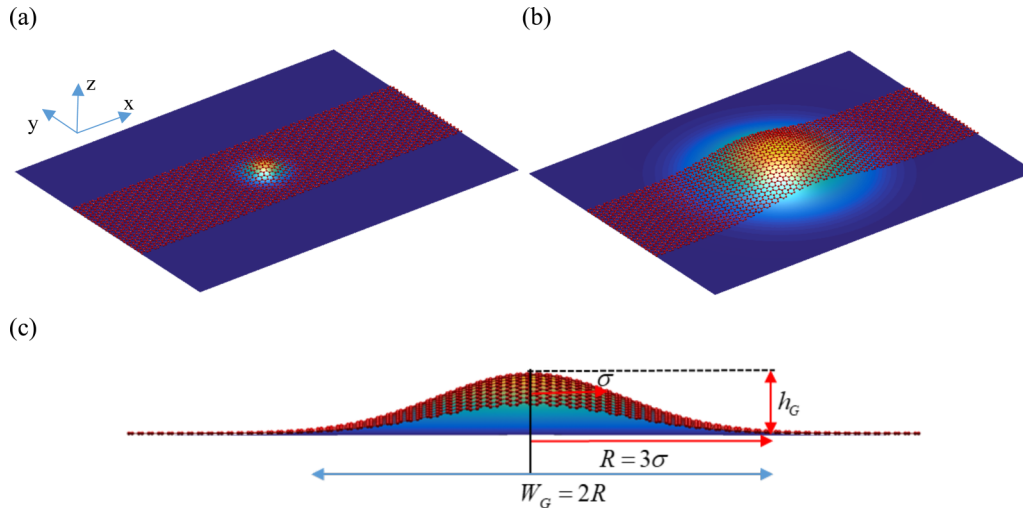
*vantruongtran.nanophys@gmail.com

(a) (b)

(c)

FIG. 1. Sketch of a ribbon with Gaussian deformation. Two typical deformations are illustrated: (a) small and (b) large Gaussian bumps. (c) Parameters defining the shape of a Gaussian bump.

sublattices A and B in the deformed region has been observed even for small deformations [26,36]. Valley-electronic filtering depending on geometrical deformation [37] and current-flow paths in the deformed region [27] have also been discussed for 2D graphene with Gaussian deformation.

Although several works have been carried out to unveil the changes in the electronic properties of graphene in the presence of Gaussian deformation, the number of studies in this topic remains modest. In particular, previous studies of quantum effects in Gaussian-deformed ribbon structures have been still limited to consideration of confinement states [31,32] and charge distribution at sublattice sites [31]. Moreover, only Gaussian bumps with the size smaller than the width of considered ribbons have been investigated. Thus, further studies are needed to understand more comprehensively the impact of the shape of Gaussian bumps on the electronic properties according to the size of ribbons. Furthermore, the impacts on electron transport in a Gaussian deformed ribbon of an external electric field and edge roughness have not yet been considered.

In this work, we aim at investigating systematically the impact of Gaussian deformation on electron transport in both armchair and zigzag graphene ribbons. The correlation between the shape of a Gaussian bump and the size of a studied ribbon will be explored. In particular, we pay attention to energy gap opening in semimetallic ribbons in order to optimize graphene-based atomistic designs suitable for a broad range of applications. In addition, the effects of an external electric field and edge roughness are also considered.

The rest of the paper is organized as follows: In Sec. II we first present the concept of Gaussian deformation in a ribbon structure and the parameters used to define the Gaussian shape and the size of a ribbon, then a tight-binding (TB) model and nonequilibrium Green's-functions (NEGF) formalism are detailed for methodology. Section III is devoted to results and discussions. In Sec. III A, a comprehensive study of the electron transport in graphene ribbons with Gaussian deformation is discussed. In Sec. III B, the effect of an external electric field on the electronic properties of Gaussian deformed

ribbons is investigated. In Sec. III C, the individual and mutual impacts of Gaussian deformation and edge roughness are presented. Finally, Sec. V concludes this paper.

II. MODEL AND METHODOLOGY

A. Model

A graphene ribbon with Gaussian deformation is illustrated in Fig. 1 for two typical sizes of Gaussian bumps: small [Fig. 1(a)] and large [Fig. 1(b)], with respect to the size of the ribbon. The bump position is illustrated with a color gradient. These two distinct Gaussian bumps may impact differently the physical properties of the ribbon including the electron transport properties.

The height of atoms within a centrosymmetric Gaussian deformed region is defined as follows [38]:

$$z(x, y) = h_G e^{-[(x-x_0)^2+(y-y_0)^2]/2\sigma^2}, \quad (1)$$

where x_0, y_0 are the x, y coordinates of the central point of the bump. In all cases, we set the peak of the bump to be on top of the center of the considered ribbon. The shape of the Gaussian bump is generally characterized by two geometrical parameters h_G and σ which are the height and the standard deviation of the Gaussian shape as illustrated in Fig. 1(c) [38]. Sometimes, the parameter $b = \sqrt{2}\sigma$ is also used to characterize the width of a Gaussian bump [31,36,37]. To compare the width of the Gaussian bump with that of the ribbon, it may be more relevant to determine the diameter of the bottom circle of the Gaussian shape on the plane of the ribbon. It is well known that the circle of radius $R = 3b/\sqrt{2} = 3\sigma$ contains 99.7% of the Gaussian bump [32]. The diameter of this circle is thus $W_G = 2R = 6\sigma$ and can be used as the bump width to be compared with the width of the ribbon.

Besides, the geometrical definition of the width of a ribbon depends on the edge orientation of the ribbon. The width of an AGNR is defined as $W_R = (M - 1) \times \sqrt{3}/2 \times a_0$, while that of a ZGNR is calculated as $W_R = (3M - 2) \times a_0/2$, where $a_0 = 1.42$ Å is the distance between two neighboring atoms

in perfect graphene structures and M is the number of dimer (chain) lines along the ribbon width of an AGNR (ZGNR) [39].

It should be noted that in the area of a Gaussian bump, the mechanical strain is nonuniform and the strain intensity inside the deformed region is defined as $\varepsilon = h_G^2/(2\sigma^2)$ [36]. On the other hand, it has been shown in previous studies [40] that for a strain intensity above 25%, graphene enters into the inelastic regime where both the mechanical and electronic properties are unpredictable. Therefore, in this work, we consider only Gaussian bumps with strain intensity less than or equal to 15%.

It is also worth mentioning that Gaussian bumps generated by rough substrates may be of a few nm in size, i.e., typically 4–10 nm wide and 0.3–2.0 nm tall [25]. The diameter of an STM tip being in the range of a few nm to 50 nm [41–43], Gaussian bumps generated by an STM process can have a width ranging from less than 1 nm to a few tens of nm. So, in this work we consider only Gaussian deformation of such width, to be consistent with experiments. Additionally, ribbons having the width of a few nm are now feasible by means of the latest technology [44,45].

B. Methodology

To investigate the electronic properties of nonuniform strain graphene structures, we employed the simple first-nearest-neighbors (1NN) TB model that has been widely used in previous works [27,31,32,36,38]. A term related to a nonzero external electric field was also added. Thus, our Hamiltonian yields

$$H = -\sum_{ij \in 1NN} t_{ij} |i\rangle\langle j| + \sum_i U_i |i\rangle\langle i|. \quad (2)$$

The hopping energy between two lattice sites ith and jth is defined as

$$t_{ij} = t_0 e^{-\beta(d_{ij}/a_0 - 1)}, \quad (3)$$

where the coefficient $\beta = 3.37$ is defined by the strain theory [46], $t_0 = 2.8$ eV is the hopping energy between the two nearest sites in the unstrained region, $d_{ij} = \sqrt{(x_i - x_j)^2 + (y_i - y_j)^2 + (z_i - z_j)^2}$ is the distance between the ith and jth sites. $U_i = -e.\vec{E} * (\vec{r_i} - \vec{r_O})$ is the electrostatic potential at the ith lattice site under an external field $\vec{E}$ and $\vec{r_O}$ is the origin of the potential.

The quantum transport properties of structures were examined by coupling the TB Hamiltonian with the NEGF technique [47]. All structures were divided into three parts: the left and right leads and the device region (central region). The leads were considered as semi-infinite regions. The device (central) region contains the left lead extension, the active region, and the right lead extension and these parts have N_L, N_A, N_R primary unit cells, respectively. The length of the device is characterized by the total number of unit cells $N = N_L + N_A + N_R$. Disorders were introduced only in the active region. It is worth noting that a primary unit cell of a ribbon contains two slices with a total of $2M$ atoms.

The Green's function of the device region was calculated as follows:

$$G = \left[E^+.I - H_D - \Sigma_L^s - \Sigma_R^s \right]^{-1}, \quad (4)$$

where $E^+ = E + i\eta$ with η is an infinitesimal positive number, H_D is the Hamiltonian of the device, and

$$\sum_L^s = H_{DL} G_L^0 H_{LD},$$

$$\sum_R^s = H_{DR} G_R^0 H_{RD} \quad (5)$$

define the surface self-energies contributed from the left and right leads. $G_{L(R)}^0$ represents the surface Green's function of the isolated left (right) lead and was computed by Sancho's technique [48]. The size of the device Green's function in Eq. (4) was reduced using the recursive technique [49]. Then electron transmission was computed as [47,50]

$$T_e = \text{Trace}\left\{ \Gamma_L^s \left[i(G_{11} - G_{11}^\dagger) - G_{11} \Gamma_L^s G_{11}^\dagger \right] \right\}, \quad (6)$$

where $\Gamma_{L(R)}^s = i(\Sigma_{L(R)}^s - \Sigma_{L(R)}^{s}{}^\dagger)$ denotes the surface injection rate at the left (right) lead. The local density of states (LDOSs) at the ith lattice site were calculated by [49]

$$D(\vec{r_i}, E) = -\frac{\text{Im}[G_{ii}(E)]}{\pi}. \quad (7)$$

III. RESULTS AND DISCUSSION

In this section, first the impact of Gaussian deformation on the electron transport properties of different groups of ribbons is analyzed in detail. Then the variation of the electronic properties of deformed ribbons under an external electric field and the presence of edge roughness is discussed.

A. Impact of Gaussian deformation on the electronic properties of ribbons

It is well known that based on the electronic features, perfect AGNRs are classified into three groups $M = 3p + 2$, $3p + 1$, and $3p$ where p is an integer number [4]. Thus, to understand precisely the impact of Gaussian deformation on the electronic properties of different types of ribbons, it is necessary to examine the effect of deformation for each of these groups.

First, we investigate AGNRs of the semimetallic group $M = 3p + 2$. In Fig. 2, the electron transmission of a device made of a semimetallic AGNR of width $M = 41$ ($W_R \approx 49.19$ Å) and length $N = 150$ unit cells ($L \approx 637.58$ Å) is shown for the perfect (undeformed) structure (black curve) and for deformed ones with several configurations of Gaussian bumps: very small ($W_G/W_R \approx 0.67$, red curve), small ($W_G/W_R \approx 0.95$, violet curve), medium ($W_G/W_R \approx 1.50$, blue curve), and large ($W_G/W_R \approx 5.63$, green curve) bumps. In all cases, strain intensity is fixed at 15%. As can be observed, the electron transmission is altered even for small Gaussian bumps (red and violet curves) where $W_G < W_R$. The degradation is more pronounced in the high-energy regions than in the low-energy region. Notably, the first step of the transmission remains almost unchanged. The effect is stronger
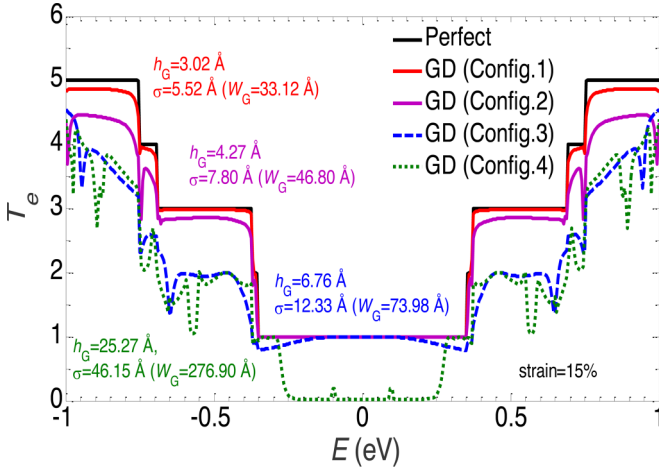
FIG. 2. Electron transmission in an AGNR without and with Gaussian deformation (GD): $M = 41$ ($W_R \approx 49.19\,\text{Å}$), $N = 150$ ($L \approx 637.58\,\text{Å}$). Different levels of deformation are considered and strain intensity is fixed at 15%.

with larger bumps. This result is in agreement with what was observed in a previous study [31]. Interestingly, when Gaussian deformation is large enough (blue, green lines) with $W_G > W_R$, the transmission at high energy is found to weakly change. However, the first plateau drops strongly around $E = 0$ and a transport gap is formed when the Gaussian bump is sufficiently large (green line). At the energy point $E = 0$, the transmission of the strongly deformed ribbon remains at only 1.6% ($T_e = 0.016$) compared to the value of 1.0 in the perfect and weakly deformed structures.

The change of the transmission at low and high energies could be, phenomenologically, understood in terms of scattering wavelength. Gaussian bumps can be considered as local defects that lead to scattering of electronic states with typical wavelengths of the size of the local defect. Therefore, small deformations corresponding to short wavelengths affect mainly high-energy electronic states, which explains the strong robustness of the first plateau of the transmission against small Gaussian deformations. Similarly, larger

deformations can scatter lower energy states of longer wavelengths. To understand better the variation of the electron properties due to the Gaussian deformation, the LDOS is plotted in Fig. 3 as a function of energy and the transport direction (ox) in real space. Figures 3(a) and 3(b) respectively present the results of the medium (Config. 3) and large (Config. 4) deformed structures are shown in Fig. 2. In Fig. 3(b), i.e., in the case of large deformation, we observe that the LDOS near the peak of the Gaussian bump (central position) around the energy $E = 0$ is strongly reduced (dark blue area) with respect to the case of small deformation presented in Fig. 3(a) (blue area).

The low LDOS in the central region can be understood as a consequence of a larger area of the deformed region. It induces more effective scattering than in the case of weakly-deformed structures and therefore smaller electrical conduction in the deformed region. This is consistent with the transmission drop around the zero energy shown in Fig. 2.

To clarify this point, we studied the bonding lengths in each considered structure. The bonding maps for the centrosymmetric Gaussian deformations Configs. 3 and 4 are respectively shown in Figs. 4(a) and 4(b). The color gradient presents the changes in the nearest bonds (1NN) with atom distance ranging from 1.42 to 1.5 Å. From these panels, it manifests that the strongest deformation occurs at the middle height of the Gaussian bumps, while the areas at the top and the leg of the bumps are weakly tensile. It is worth noting that the profile of bonds in Fig. 4(a) leads to a sixfold region with low LDOSs which is similar to the flower shape observed in the previous study [31].

From the calculated bonding length, the nearest hopping energy of each bond was deduced by using Eq. (3). In Figs. 4(c) and 4(d) the profile of the hopping energies of all bonds at their bonding positions along the transport direction is shown for the two considered structures. The coordinates of a bond between the ith and jth atoms were simply defined as $\vec{r}_{t_{ij}} = (\vec{r}_i + \vec{r}_j)/2$. Interestingly, the shape of these two hopping profiles is remarkably different and can be used to interpret the physics involved in the behavior of the corresponding transmissions shown in Fig. 2. Figure 4(c) indicates
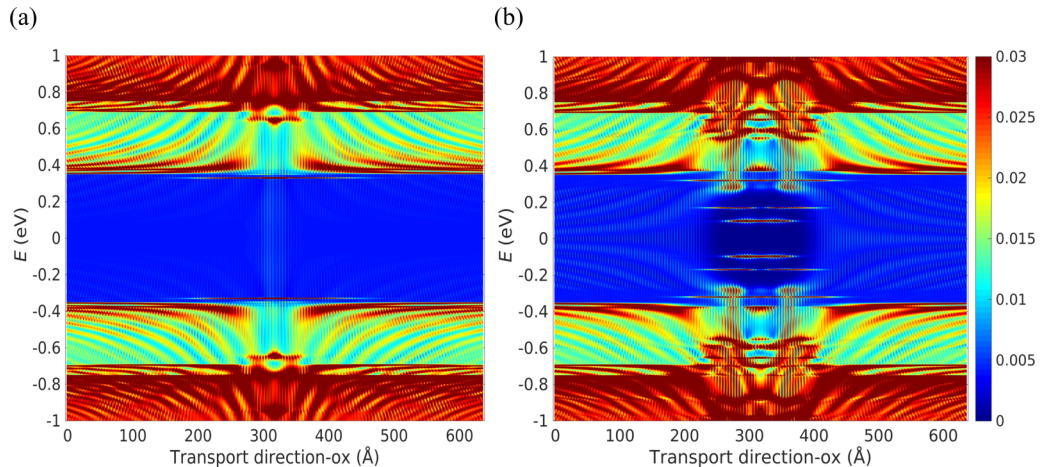

FIG. 3. LDOS (in arbitrary units) as a function of energy and transport direction (ox) for two deformations: $h_G = 6.67\,\text{Å}$, $\sigma = 12.33\,\text{Å}$ (Config. 3) and $h_G = 25.27\,\text{Å}$, $\sigma = 46.15\,\text{Å}$ (Config. 4). $M = 41$ ($W_R \approx 49.19\,\text{Å}$), $N = 150$ ($L \approx 637.58\,\text{Å}$).
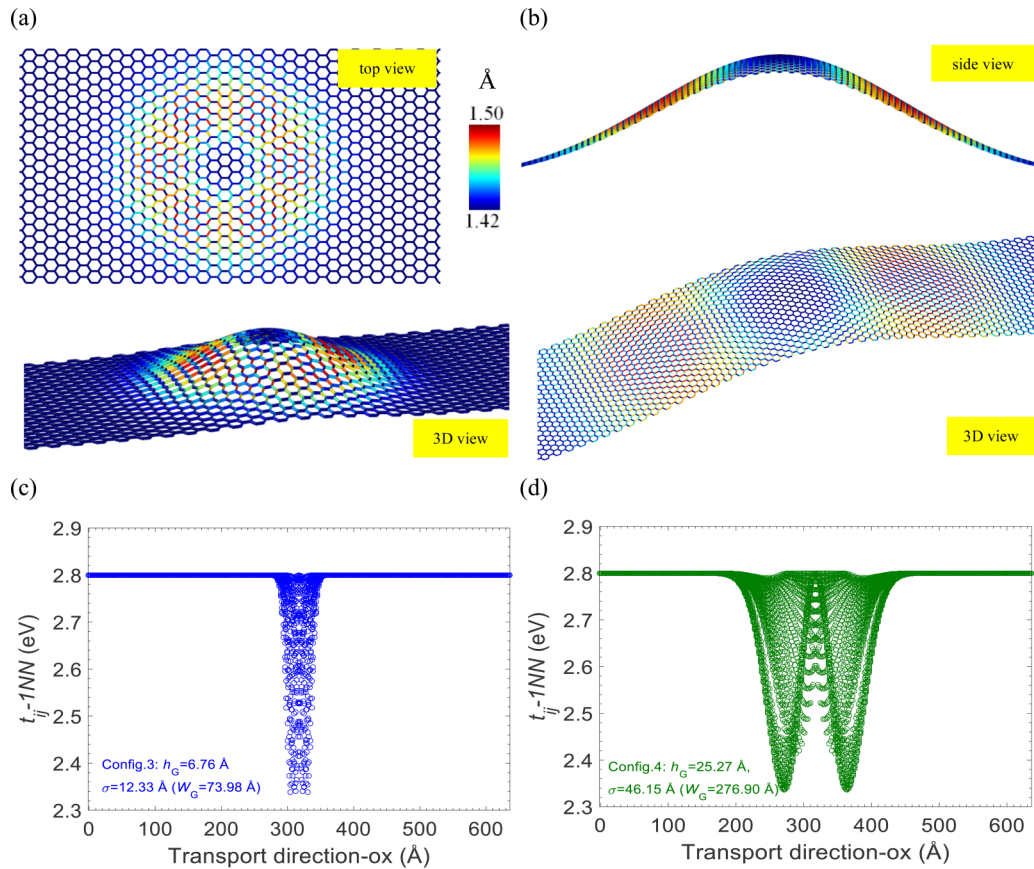
FIG. 4. Bonding length map and hopping profile in the ribbon with two different centrosymmetric Gaussian deformed configurations: (a),(c) $h_G = 6.67$ Å, $\sigma = 12.33$ Å (Config. 3) and (b),(d) $h_G = 25.27$ Å, $\sigma = 46.15$ Å (Config. 4). Here $M = 41$ ($W_R \approx 49.19$ Å), $N = 150$ ($L \approx 637.58$ Å).

that in the weakly deformed structure, a single nonuniformed region is formed around the top of the Gaussian bump where the hopping energies are reduced. Similar hopping profiles are obtained for Configs. 1 and 2. Differently, in the case of strong deformation, three nonuniformed regions are formed inside the Gaussian bump as the standard hopping energy region near the peak is sandwiched in between two low hopping energy regions. The electron transport between regions of different hopping energies is limited and even blocked in the case of strong deformation. Indeed, in such a three-region system which is similar to a double-barrier potential profile, the presence of scatterings at each region interface and also quantum trapping in the "pseudowell" limit the electron transport. That explains the low transmission in the low-energy region for the Config. 4 observed in Fig. 2. Moreover, the difference between the hopping profiles of Configs. 3 and 4 stems from the correlation between the shape of the Gaussian bump and the size of the ribbon. In Config. 3, the hopping profile along transport direction [Fig. 4(c)] shows that hopping energies in the region around the peak of the Gaussian bumps are similar to the those of the regions on the two sides of the peak and there is a significant increase of some bonding lengths along the y direction in this region [Fig. 4(a)]. In contrast, if the Gaussian bump along the y direction covers the full width of the ribbon [Fig. 4(b)], the region around the peak of the large deformed structure contains only weakly stressed bonds and thus hopping energies are remarkably different

from those in the two regions on the sides on the peak [Fig. 4(d)].

In summary, when the deformation is distributed over the entire width of the ribbon, the low-energy electrons cannot cross the slightly deformed regions near the edges as in Config. 3 [see Fig. 4(a)]. Thus a transport gap is observed when the Gaussian bump is large enough so that the hopping profile of the deformed region clearly shows a three-zone characteristic.

To further analyze the dependence of the transmission on the level of deformation, and particularly to find out the crucial condition to observe a transport gap around the zero-energy point, we investigated the variation of the transmission at $E = 0$ for different configurations of Gaussian deformation. As the shape of a Gaussian bump depends not only on the height h_G but also the width σ or W_G, it is relevant to consider these two parameters. Additionally, the transport properties also depend on the ribbon width W_R, so it can be more relevant to consider the correlation between the shape of the Gaussian bump and that of the ribbon. We found that the ratio $h_G W_G / W_R$ is the most relevant parameter to be used to establish a correlation between the sizes of the ribbon and the bump. In Fig. 5, $T_e(E = 0)$ is plotted as a function of the ratio $h_G W_G / W_R$ for different ribbon sizes and also different levels of strain induced by Gaussian deformation.

As can be observed in the left inset of Fig. 5, all the transmission curves drop almost exponentially. Interestingly,
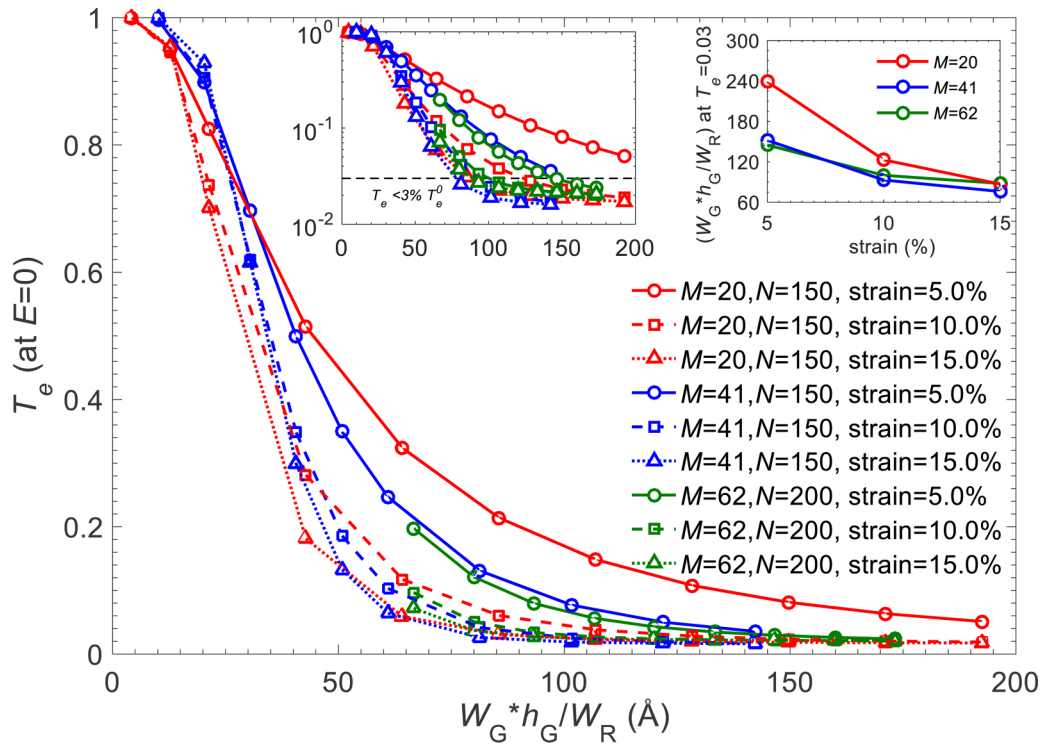
FIG. 5. Correlation between T_e at $E = 0$ and the ratio $h_G W_G / W_R$. Left inset is the result that T_e is in the logarithmic scale and the horizontal dashed line in this inset indicates that 97% transmission is suppressed. Right inset shows the cutoff ratio $h_G W_G / W_R$ at $T_e = 0.03$ of each curve shown in the main panel.

these curves tend to converge at a large value of the ratio $h_G W_G / W_R$. It is shown in the left inset that below the horizontal dashed line, the transmission is reduced by 97% confirming that an effective transport gap is formed when the shape of the Gaussian bump is large enough. For each configuration, the ratio $h_G W_G / W_R$ leading to this transmission reduction of 97% (i.e., at $T_e = 0.03 * T_e^0$) was determined by performing a spline fitting. The results are shown in the right inset of Fig. 5. It can be observed that the ratio to reach the transmission threshold of $0.03 * T_e^0$ depends on both the ribbon width and the level of strain while the latter is associated directly with the shape of the Gaussian bump. Besides, when ribbons are large enough and the strain is significant (equal to or larger than 15%), the required ratio seems to converge to a value of about 80 Å.

It is worth noting that the large centrosymmetric Gaussian deformed structure (bump) shown in Fig. 4(b) is similar to a ribbon with a Gaussian fold where the height of an atom in the deformed region is defined as $z(x, y) = h_G e^{-(x-x_0)^2/2\sigma^2}$. This type of Gaussian deformation generates a fold along the y direction. Such a deformation has been discussed recently about valley filtering properties [37] and Kondo effect under a magnetic impurity in 2D graphene structures [29]. To understand if the formation of a transport gap is also observed in graphene ribbons with this kind of Gaussian deformation, we examined the electronic properties of several Gaussian fold deformed ribbons. The obtained results are displayed in Fig. 6. Figure 6(a) presents the transmission of a ribbon of width $M = 41$ ($W_R \approx 49.19$ Å) and length $N = 150$ ($L \approx 637.58$ Å) for four different Gaussian fold configurations as displayed in this panel. As can be observed in Fig. 6(a), with

the same Gaussian shape parameters, the transmission of a Gaussian fold deformed structure is degraded more strongly compare to that of its Gaussian bump counterpart (shown in Fig. 2). This can be understood as the Gaussian fold with the same Gaussian parameters has a larger deformed surface compared to the similar Gaussian bump [see insets of Figs. 6(c) and 4(a)]. Transmission at $E = 0$ is also found to drop exponentially as in the case of the Gaussian bumps as shown in Fig. 6(b). However, to achieve a transmission reduction of 97% in the case of Gaussian folds, weaker deformation than that in the case of bumps is required. Indeed, for instance in the case of 10% of strain and a ribbon of width $M = 41$, the crucial ratios $h_G W_G / W_R$ are equal to 67 Å for the fold and 93 Å for the bump. An analysis of the hopping profiles in these structures with Gaussian fold seen in Figs. 6(c) and 6(d) gives behavior similar to those related to the Gaussian bumps, i.e., a transport gap is observed when the hopping profile exhibits clearly a three-zone characteristic. It should be noted that the hopping profile of a Gaussian fold ribbon is different from that of a Gaussian bump ribbon because at a given x coordinate, the deformation along the y direction is uniform in this type of deformed structures as can be seen in the inset of Fig. 6(c). Such difference also leads to the three-zone behavior in the hopping profile of the small folds [Fig. 6(c)], although, it is still less visible.

Thus, qualitatively the impact of Gaussian bumps and folds on the electron transport properties of graphene ribbons is similar. Therefore, only deformations with Gaussian bumps are discussed further hereafter.

To understand the effect of Gaussian deformation on the electronic properties of semiconducting AGNRs (groups $3p +$
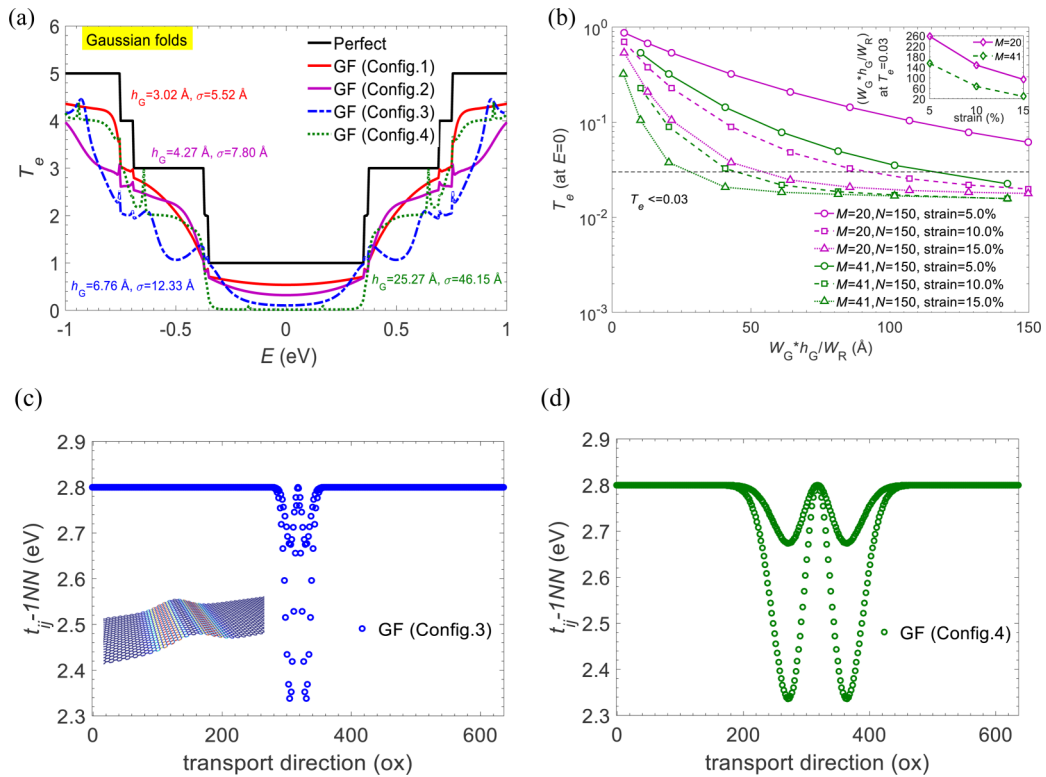
FIG. 6. Gaussian folds (GF): (a) T_e as a function of energy for several GF configurations in the ribbon of width $M = 41$ ($W_R \approx 49.19$ Å), and length $N = 150$ ($L \approx 637.58$ Å). (b) Correlation between T_e (at $E = 0$) and the ratio $h_G W_G / W_R$. (c),(d) Hopping profiles in the ribbon with the GF Configs. 3 and 4 presented in panel (a). Inset in panel (b) presents the cutoff ratio $h_G W_G / W_R$ at $T_e = 0.03$ as a function of strain for different ribbon widths. Inset in panel (c) is the bonding map of the GF Config. 3, the color bar is from 1.42 Å to 1.5 Å as in Fig. 4.

1 and $3p$), we examined a ribbon of width $M = 39$ ($W_R \approx 46.73$ Å) which belongs to the $3p$ group. The results are shown in Fig. 7 for different shapes of Gaussian deformation (Gaussian bumps). Similar results were obtained for the $3p + 1$ group (not shown).

As can be seen in Fig. 7, around the first step of the "perfect" transmission (black line), in the presence of Gaussian deformation, transmission decreases and the reduction is stronger with larger Gaussian bumps. Interestingly, with the largest Gaussian deformation considered here, the band gap seems to be enlarged (green line). For transmission at higher transmission steps, we also observe a strong reduction
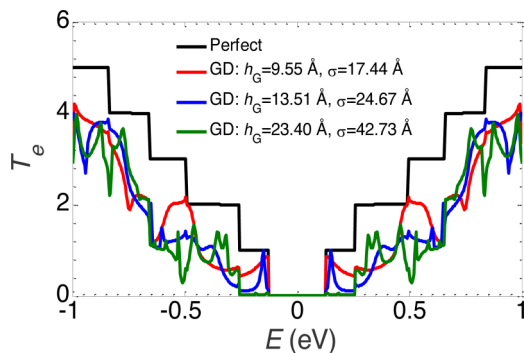

FIG. 7. Semiconducting armchair with several configurations of centrosymmetric Gaussian deformation (GD): T_e vs E. Here $M = 39$ ($W_R \approx 46.73$ Å), $N = 150$ ($L \approx 637.58$ Å).

for all studied cases. Additionally, the behavior is similar to that of semimetallic ribbons in which the high-energy transmission of the deformed structures is less dependent on the level of deformation. Our analyses showed that the variation of transmission at the low-energy region around $E = 0$ is similar to that of the semimetallic group ($M = 3p + 2$) as discussed above, i.e., the transport gap is only widened when the hopping profile presents three nonuniformed zones along the transport direction in the deformed region.

To complete the examination of the different types of ribbons, we now consider Gaussian deformation in ZGNRs. In Fig. 8, the results of the electron transmission of a zigzag structure of width $M = 20$ chain lines ($W_R \approx 41.18$ Å) are shown. Similar results were obtained for other ZGNRs. As can be seen in Fig. 8(a), the transmission without and with Gaussian deformation displays a reduction of the electron transport near the first step of the transmission. However, the first plateau remains unchanged even with a strong deformation (dot blue line). Thus there is no band-gap opening in ZGNRs under Gaussian deformation. This phenomenon can be understood by looking at the total density of states (TDOSs) in the device. The TDOSs without and with deformations are shown in Fig. 8(b). It can be seen that the middle peak of the TDOSs localizes at the energy $E = 0$ and it is unchanged with the deformation. This peak actually corresponds to the strongly localized edge states in the zigzag ribbon [3]. Due to the presence of edge states in the low-energy region, even for strong deformations a transport gap cannot be opened. It is also worth
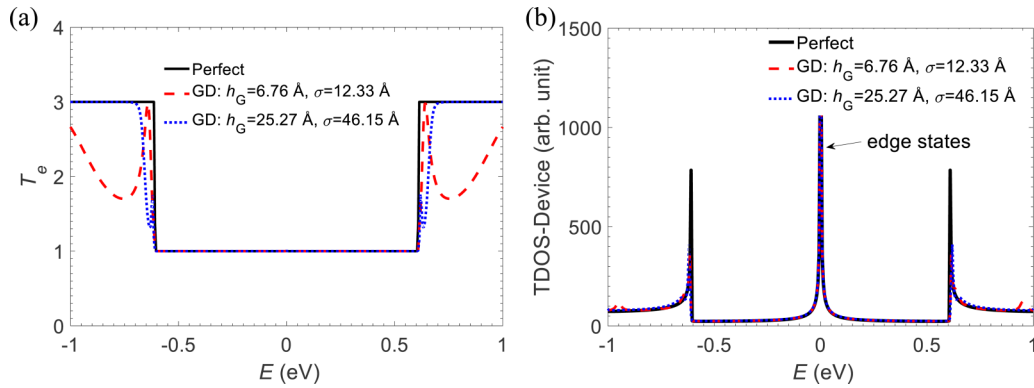
FIG. 8. (a) Transmission and (b) TDOS of a device made of a ZGNR of width $M = 20$ ($W_R \approx 41.18\,\text{Å}$), $N = 150$ ($L \approx 367.69\,\text{Å}$).

mentioning that a transport gap around $E = 0$ can be opened in the zigzag-edge graphene systems with multiple terminals due to the quantum interference in the central region [51].

B. Asymmetrical effect of a vertical electric field on Gaussian deformed ribbons

It has been demonstrated that external electric fields can be used to modulate the electronic properties of materials and devices [2,52,53]. It has been shown in previous studies [52,54,55] that a transverse (positive or negative) electric field modulates symmetrically the conduction and valence bands. This phenomenon stems from the mirror symmetry of ribbons about an axis located in the middle of ribbons. A similar effect has also been observed in bilayer structures with a vertical electric field [2,56].

In the presence of a Gaussian deformation, the mirror symmetry in the transverse plane (xy plane) is not affected but this symmetry in the vertical planes is broken. Thus some asymmetrical effects could be observed if a vertical electric field was applied.

To verify this prediction, we first examined the effect of a transverse electric field $\overrightarrow{\text{E}} = E_y \overrightarrow{e_y}$ in a Gaussian deformed AGNR of width $M = 41$ (group $3p + 2$) and length $N = 150$. It is worth mentioning that a transverse electric field can be generated by two side gates at the edges of the system. The

fabrication of such gates could be done by using electron-beam lithography and thermal evaporation [57]. For different external fields, the transmission is plotted as a function of the energy in Fig. 9(a). The results without any external field for the perfect and deformed structures are also displayed for comparison. As can be seen, the transverse electric field remarkably impacts the electron transport, particularly in the low-energy region around $E = 0$. This electric field acts symmetrically on the conduction and valence bands. Additionally, as observed in standard ribbons [58], the sign of the field is not relevant, only the norm of the field matters.

It is worth noting that within a more sophisticated TB model up to third-nearest neighbors and with overlap factors, the conduction and valence bands are not perfectly symmetrical [39]. However, in TB models an external field modifies only the on-site energy of atoms and it induces an effect on both conduction and valence bands, thus the change attributed to the external fields does not depend on the chosen TB model. Also, as the studied device sizes are significantly large (from a few thousand to more than ten thousands of atoms), to avoid a computationally demanding self-consistent process, fields lower than 20 mV/Å were considered and charge redistribution in such large ribbons was neglected.

To check the effect of a vertical electric field $\overrightarrow{\text{E}} = E_z \overrightarrow{e_z}$, the transmissions computed for both $+E_z$ and $-E_z$ are shown
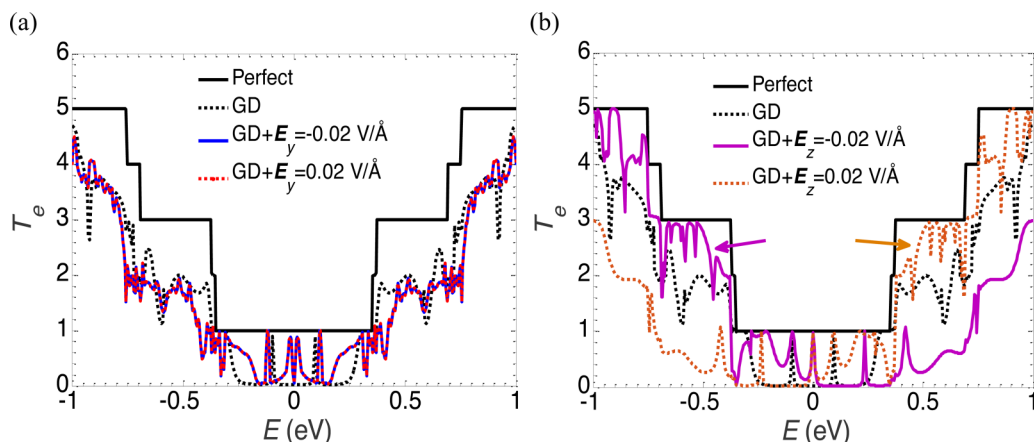

FIG. 9. An AGNR of width $M = 41$ ($W_R \approx 49.19\,\text{Å}$) and length $N = 150$ ($L \approx 637.58\,\text{Å}$) with a large Gaussian deformation (GD) $h_G = 25.27\,\text{Å}$, $\sigma = 46.15\,\text{Å}$ under the effect of (a) a transverse electric field $\overrightarrow{\text{E}} = E_y \overrightarrow{e_y}$ and (b) a vertical electric field $\overrightarrow{\text{E}} = E_z \overrightarrow{e_z}$.
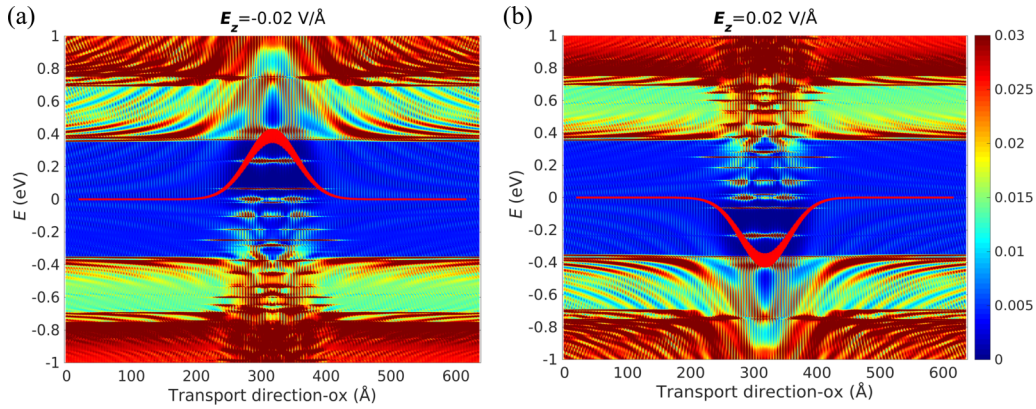
FIG. 10. LDOS vs E-ox for opposite fields (a) $E_z = -0.02\,\text{V/Å}$ and (b) $E_z = 0.02\,\text{V/Å}$. Red lines are electrostatic potential profiles induced by the electric fields. Here $M = 41$ ($W_R \approx 49.19\,\text{Å}$), $N = 150$ ($L \approx 637.58\,\text{Å}$), and the Gaussian bump $h_G = 21.36\,\text{Å}$, $\sigma = 39.01\,\text{Å}$. In both panels, LDOS is in arbitrary units.

in Fig. 9(b). Interestingly, as predicted, an asymmetrical effect on the conduction and valence bands is observed with both $+E_z$ (orange curve) and $-E_z$ (violet curve). Under a $+E_z$ field, the electron transport in the conduction range is significantly enhanced (compared to the case without electric fields). In contrast, the transmission in the valence band is reduced. It is also worth noting that the transport gap is shifted to the position below the energy point $E = 0$. Furthermore, the effect of the $-E_z$ field is reversed, i.e., an enhancement of the transmission in the valence band and a reduction in the conduction band, as seen in Fig. 9(b).

This asymmetrical effect of the vertical electric field on the electron transmission may be interesting for several applications such as energy filters, rectification devices, or sensors.

To better understand the effect of opposite vertical electric fields, we plotted in Fig. 10 the LDOS as a function of energy and the transport direction. The red lines in Fig. 10 display the electrostatic potential at each lattice site along the transport direction. As can be seen in Fig. 10(a), under the effect of the $-E_z$ field, a barrier potential (red line) is established and it causes additional scattering in the region of positive energies. As a consequence, the transmission in the positive energy region drops, as indicated by the violet curve in Fig. 9(b). Besides, this potential profile shifts up states below the barrier, leading to an enhancement of the LDOS in the negative energy region, in particular at high energies in this region [Fig. 10(a)]. This explains the enhancement of the electron transport in the negative energy region, as indicated by the violet arrow in Fig. 9(b). It is worth noting that also due to the presence of the potential barrier, there are some strong confinement states within the barrier as seen in Fig. 10(a) and it leads to additional sharp peaks in the transmission near the original two central peaks around $E = 0$ as seen on the violet curve in Fig. 9(b). When the field has the opposite direction ($+E_z$), a quantum well is formed, as shown by the red curve in Fig. 10(b), and the phenomenon is reversed compared to the case of the field $-E_z$. Similar results were also observed for other groups of armchair ribbons $M = 3p + 1, 3p$.

We also considered the effect of a vertical electric field on the electronic properties of deformed zigzag ribbons. Similar to the case of armchair ribbons, an enhancement of the electron transmission was also observed in the conduction region when applying a $+E_z$ field (red line) compared to the case without the field (blue line) as indicated by arrows in Figs. 11(a) and 11(b). And we also observed an inverse effect for the field $-E_z$.

Interestingly, a transport gap in the zigzag structure appears with an even number of chain lines M as shown from the red line in Fig. 11(b). But such a result is not obtained for the odd M zigzag ribbon in Fig. 11(a). In fact, this even-odd effect originates from the well-known parity effect of wave functions in ZGNRs in which the electron transmission is blocked if the right- (left-)going states $+\vec{k}$ ($-\vec{k}$) of different channels at the same energy level have a different parity [59,60]. The potential induced by the external field leads to a shift of the energy bands in the active region, which results in opposite parities of wave functions and causes a drop of transmission in even M zigzag ribbons [59,60].

C. Edge roughness in Gaussian deformed ribbons

In fabricated ribbons, the edges are commonly not perfect in particular in ribbons made by top-down techniques [6]. It has been also demonstrated that edge roughness strongly impacts on the electronic properties of ribbons [10,15]. In this section, we examine the variation of the electron transport of deformed ribbons in the presence of edge roughness.

To generate edge roughness in a ribbon, N_{vac} atoms were randomly removed from edges, i.e., N_{vac} interactions were processed and for each one of them a random atom at a random edge was chosen to be removed. It should be noted that the random process can remove atoms in the second line or even in other internal lines from the edges if some border atoms were removed in previous random steps. The level of edge roughness can be defined by the probability to remove atoms at the two edges $P_{\text{ER}} = N_{\text{vac}}/(4N_A)$. The coefficient 4 is because each unit cell of the perfect structure has four atoms at the two edges.

The electron transmission in different structures is shown in Fig. 12: one with a Gaussian bump, one with edge roughness and a structure with both Gaussian deformation and edge roughness. Two cases of Gaussian deformation where a small [Fig. 12(a)] and a large [Fig. 12(b)] Gaussian bumps
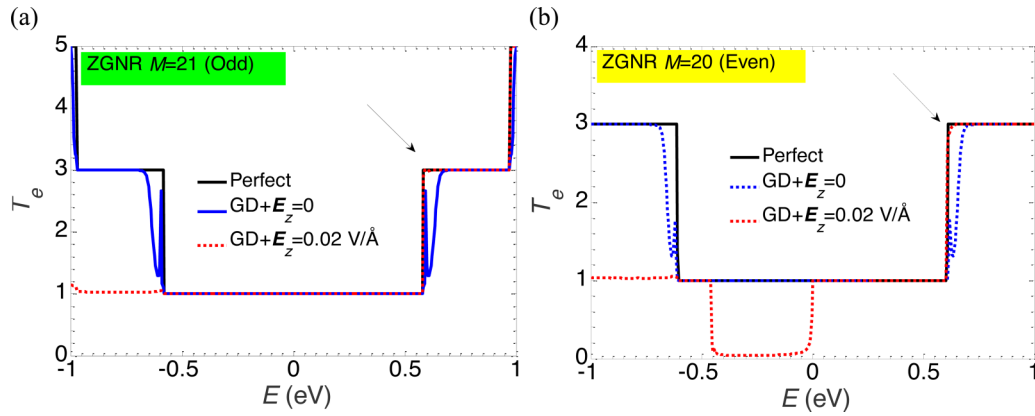
FIG. 11. Transmission of ZGNRs without and with a vertical field. (a) Results for odd $M = 21$ ($W_R \approx 43.31\,\text{Å}$), $N = 150$ ($L \approx 367.69\,\text{Å}$). (b) Results for even $M = 20$ ($W_R \approx 41.18\,\text{Å}$), $N = 150$ ($L \approx 367.69\,\text{Å}$). Both ZGNRs have Gaussian deformation (GD) with the same size $h_G = 25.28\,\text{Å}$, $\sigma = 46.15\,\text{Å}$.

were considered. In both cases, 5% of edge roughness was considered.

It is worth mentioning that the detailed profile of the transmission of rough ribbons depends on the specific edge-roughness configuration that is stochastic. Thus the transmission should be averaged over many edge configurations. However, as the overall behavior is the same, the results of only one configuration are shown here.

In both Figs. 12(a) and 12(b), it can be observed that the edge disorder (blue lines) suppresses the electronic transmission more strongly than the Gaussian deformation (red lines). When these two effects are combined, the obtained transmission is dominated by the edge-roughness effect (see green lines). Interestingly, the mutual effect leads to a stronger reduction of the transmission at high-energy regions. In contrast, the transport of electrons in the low-energy region near
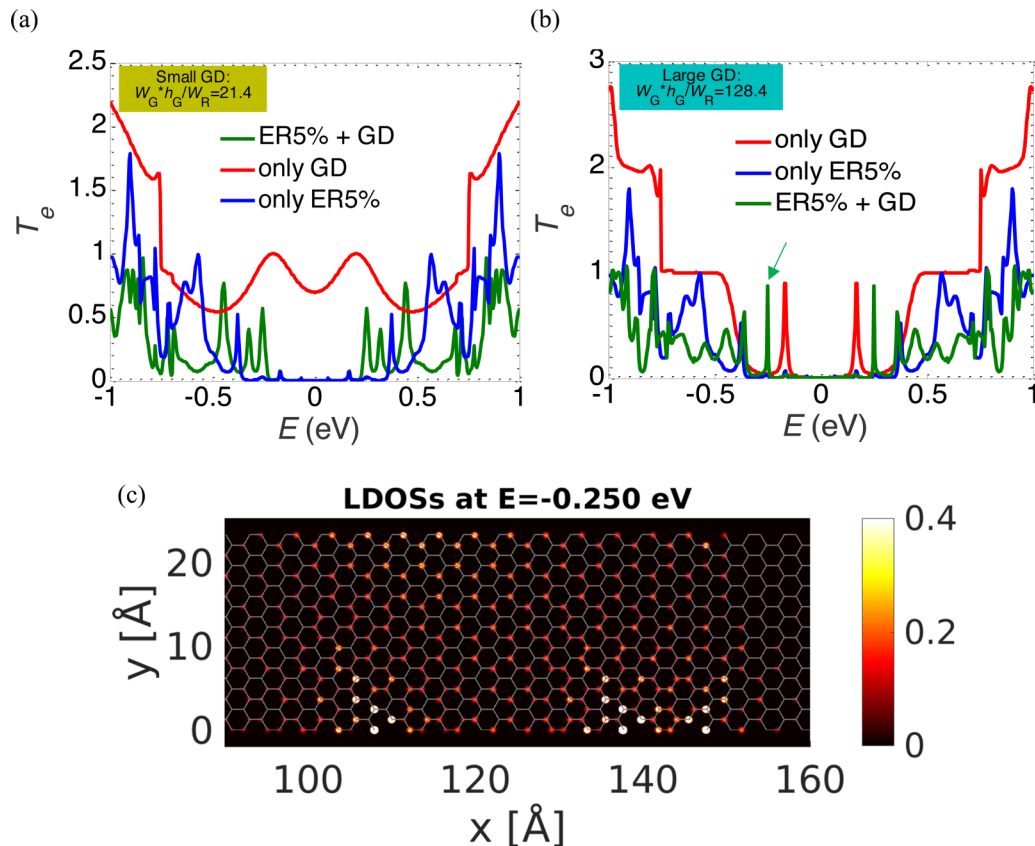

FIG. 12. Transmission of a AGNR $M = 20$ ($W_R \approx 23.37\,\text{Å}$), $N = 60$ ($L \approx 254.18\,\text{Å}$). Individual and mutual effects of Gaussian deformation (GD) and edge roughness (ER) are considered. The structure with (a) small Gaussian bump $h_G = 6.76\,\text{Å}$, $\sigma = 12.33\,\text{Å}$, (b) large Gaussian bump $h_G = 16.55\,\text{Å}$, $\sigma = 30.21\,\text{Å}$. In both panels, 5% of ER was considered. (c) The LDOS (in arbitrary units) at $E = -0.25\,\text{eV}$ corresponding to the peak (indicated by a green arrow) in the green line in Fig. 12(b).
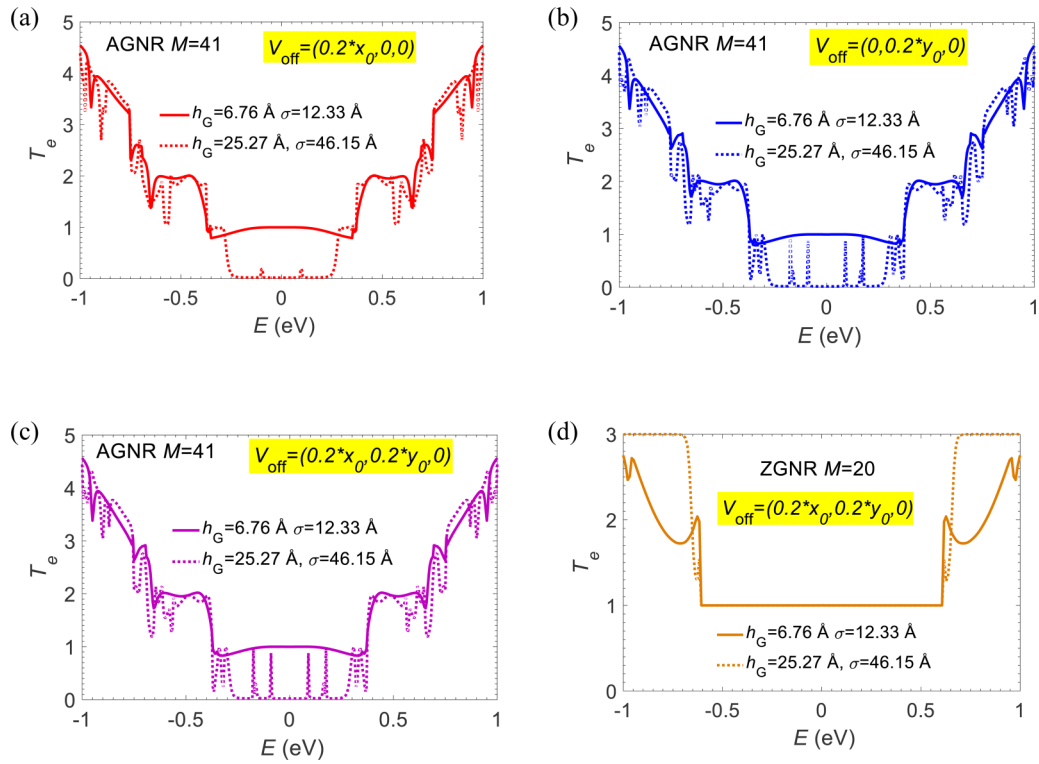
FIG. 13. Electron transmission with different positions of Gaussian bumps: results for an AGNR of width $M = 41$ with the bump is shifted (a) towards an edge, (b) along the ribbon axis, and (c) off-centered for both x and y coordinates. (d) Results of a ZGNRs of width $M = 20$. In all the panels, solid and dotted lines present results of the small and large deformations, respectively.

$E = 0$ is better than in the case where edge roughness is included, with additional transmission peaks appearing near the zero-energy point (see green lines). Such a phenomenon is due to the formation of some strong Anderson-type localized states at the locations of edge defects [14]. In Fig. 12(c) is shown the LDOS in real space of the state at $E = -0.25$ eV corresponding to the peak near $E = 0$ in the green line in Fig. 12(b), indicated by a green arrow. The result clearly shows that the positions with the highest LDOS (the brightest color) are localized at the areas of edge defects.

It should be mentioned that similar results were observed for other groups $3p$, $3p + 1$ of armchair and also zigzag ribbons (not shown).

D. Off-centered and imperfect Gaussian bumps

In practice, Gaussian bumps may not be at the center of the considered ribbon and also not perfectly in a Gaussian shape due to some possible distortion on the surface of the ribbon. Therefore, it could be relevant to consider these factors in this investigation of the effect of Gaussian deformations on the electron transport in graphene ribbons.

1. Off-centered Gaussian bumps

We first considered the impact of the off-centered Gaussian bumps. Three possible scenarios were explored where the bump is shifted from the ribbon center: (i) towards an edge; (ii) along the ribbon axis; (iii) to a general point. The off-centered position of the bump from the center of the ribbon can be defined by a vector $V_{off} = (\Delta x_G, \Delta y_G, 0)$.

Figures 13(a)–13(c) show the results of the transmission for two typical centrosymmetrical bumps of either small (solid lines) or large (dotted lines) size for an armchair ribbon structure of width $M = 41$ with three off-centered bump configurations $V_{off} = (0.2x_0, 0, 0)$, $V_{off} = (0, 0.2y_0, 0)$, and $V_{off} = (0.2x_0, 0.2y_0, 0)$, respectively. As can be observed in Fig. 13(a), the transmissions of the off-centered bumps shifted along the ribbon axis, for both small and large deformation, are almost the same as the ones of the ribbon with the central Gaussian bump, as shown in Fig. 2. When the bump is positioned near an edge of the ribbon, the small deformation has the same impact as the one at the center as can be seen from the solid blue line in Fig. 13(b). Even if the small deformation covers the edge that it is nearby, a transport gap is not observed. This result reinforces the argument that a transport is opened only when the deformation is large enough to cover the full width of the ribbon.

For the large deformation considered in Fig. 13(b) the transmission is overall similar to that in the case of the central or off-centered bump along the ribbon axis, however, with some more pronounced peaks around $E = 0$. These peaks correspond to some confined states in the deformed region as shown in Fig. 13(b). When the peak of the Gaussian bump is shifted along both x and y coordinates, the transmission is similar to that of the cases of bump shifted towards an edge [Fig. 13(b)], as seen in Fig. 13(c). Similar results are obtained for other AGNRs. It is also worth mentioning that further investigations (not shown here) indicated that the hopping profiles of small and large deformed structures are similar to that shown in Figs. 4 and 6.
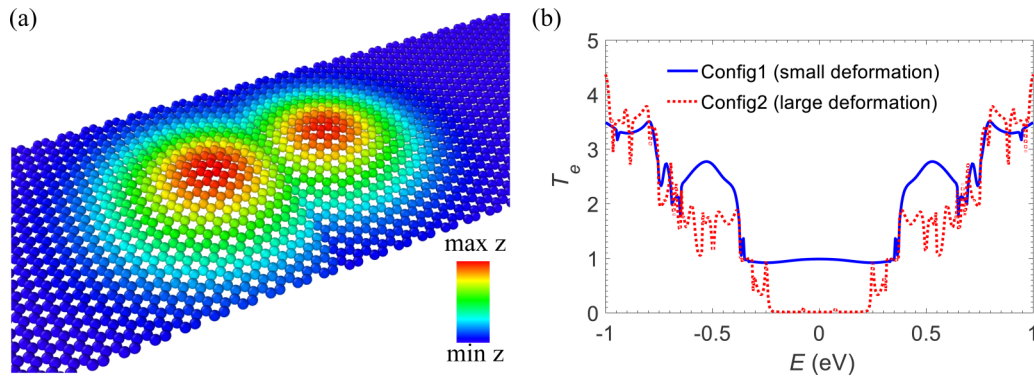
(a)

(b)

FIG. 14. (a) Illustration of an imperfect Gaussian deformation made by a mixing of two close Gaussian bumps; one is at the ribbon center and the other is off-centered at $V_{off} = (x_0/15, y_0/15, 0)$. The color gradient presents the height of atoms. (b) Electron transmission of two configurations of deformation—small (Config. 1): $h_{G1} = 5.48$ Å, $\sigma_1 = 10$ Å, $h_{G2} = 5.59$ Å, $\sigma_2 = 11$ Å; and large (Config. 2): $h_{G1} = 27.39$ Å, $\sigma_1 = 50$ Å, $h_{G2} = 27.66$ Å, $\sigma_2 = 51$ Å.

In Fig. 13(d), the results for the even-M ($M = 20$) ZGNR are displayed. As can be seen, the off-centered bumps also do not induce a transport gap as in the case of the central bump. The same behavior is observed for odd-M ZGNRs. This implies that edge states at $E = 0$ strongly localized at the edges of ZGNRs regardless of the position of deformation.

2. Imperfect Gaussian bumps

To investigate the impact of imperfect Gaussian bumps, we generated deformations with two close Gaussian bumps. The combination of the different bumps breaks the centrosymmetry of a perfect Gaussian and induces some distortion on the surface. Bumps with a slight difference in the size were used to ensure a smoothness on the surface. Such deformation is illustrated in Fig. 14(a) with the color gradient corresponding to the height of atoms. The results for weak and strong imperfect Gaussian deformation are shown in Fig. 14(b) and the overall characteristics of the transmission profiles are similar to that of the perfect Gaussian bumps shown in Fig. 2.

In summary, off-centered and imperfect-Gaussian factors only cause minor effects: the electron transmission of structures containing off-centered and imperfect Gaussian bumps is essentially similar to that of structures with central and perfect Gaussian bumps. This result suggests that the shape of an out-of-plane deformation might matter but its size correlated to the ribbon width is more essential. Hence, a study based on perfect Gaussian functions could be applied for other types of out-of-plane deformations.

IV. CONCLUSION

We have studied the electron transport properties in graphene nanoribbons with Gaussian deformation. Both

small and large Gaussian bumps with respect to the size of studied ribbons have been considered. It has been shown that Gaussian deformation strongly modifies the electronic properties of all types of ribbon structures. It leads to a strong reduction of electron transmission in high-energy regions. In the low-energy region and at the first plateau of transmission in semimetallic armchair ribbons, the transmission is just weakly affected by small Gaussian deformations, however, it drops significantly in the presence of large Gaussian bumps. Besides, the electron transmission can be reduced by 97% in structures exhibiting a sufficiently high ratio $h_G W_G / W_R$ considering the shape of the Gaussian bump over the size of the ribbon. Regarding semiconducting ribbons, the gap is enlarged when large deformations are applied. The origin of the opening or the widening of the transport gap in large deformed armchair structures has been correlated with the hopping energy profile, i.e., a formation of a three-zone behavior in the hopping profile along the transport direction. Similar electronic characteristics have been observed in the Gaussian folded ribbons. No transport gap is found in deformed zigzag ribbons due to the strong localization of edge states at the energy point $E = 0$. Furthermore, when applying a vertical electric field $+E_z$, the presence of a Gaussian bump breaks the mirror symmetry in vertical planes leading to an enhancement of the electron transport in the conduction region and a degradation in the valence zone. The effect is reversed when employing an opposite field $-E_z$. The study also unveils that the electronic behavior of the deformed ribbon including edge roughness is dominated by the characteristics of edge roughness in which strong sharp peaks in the transmission profile show strong Anderson localization. All these features are preserved when Gaussian bumps are not positioned at the ribbon center or have an imperfect Gaussian shape.

[1] F. Schwierz, Nat. Nanotechnol. **5**, 487 (2010).

[2] A. H. Castro Neto, N. M. R. Peres, K. S. Novoselov, and A. K. Geim, Rev. Mod. Phys. **81**, 109 (2009).

[3] K. Nakada, M. Fujita, G. Dresselhaus, and M. S. Dresselhaus, Phys. Rev. B **54**, 17954 (1996).

[4] L. Yang, C.-H. Park, Y.-W. Son, M. L. Cohen, and S. G. Louie, Phys. Rev. Lett. **99**, 186801 (2007).

[5] F. Tseng, D. Unluer, M. R. Stan, and A. W. Ghosh, Nanosci. Technol. **57**, 555 (2011).

[6] J. M. Marmolejo-Tejada and J. Velasco-Medina, Microelectron. J. **48**, 18 (2016).

[7] H. Sevinçli, C. Sevik, T. Caın, and G. Cuniberti, Sci. Rep. **3**, 1228 (2013).

[8] P. Dollfus, V. H. Nguyen, and J. Saint-Martin, J. Phys.: Condens. Matter **27**, 133204 (2015).

[9] V.-T. Tran, J. Saint-Martin, P. Dollfus, and S. Volz, Sci. Rep. **7**, 2313 (2017).

[10] A. Cresti, N. Nemec, B. Biel, G. Niebler, F. Triozon, G. Cuniberti, and S. Roche, Nano Res. **1**, 361 (2008).

[11] F. Mazzamuto, J. Saint-Martin, V. H. Nguyen, C. Chassat, and P. Dollfus, J. Comput. Electron. **11**, 67 (2012).

[12] Z. Kan, M. Khatun, and A. Cancio, J. Appl. Phys. **125**, 164305 (2019).

[13] D. A. Areshkin, D. Gunlycke, and C. T. White, Nano Lett. **7**, 204 (2007).

[14] G. Schubert, J. Schleede, and H. Fehske, Phys. Rev. B **79**, 235116 (2009).

[15] H. Sevinçli and G. Cuniberti, Phys. Rev. B **81**, 113401 (2010).

[16] K. Takashima and T. Yamamoto, Appl. Phys. Lett. **104**, 093105 (2014).

[17] C. P. Chang, B. R. Wu, R. B. Chen, and M. F. Lin, J. Appl. Phys. **101**, 063506 (2007).

[18] L. Sun, Q. Li, H. Ren, H. Su, Q. W. Shi, and J. Yang, J. Chem. Phys. **129**, 074704 (2008).

[19] Y. Lu and J. Guo, Nano Res. **3**, 189 (2010).

[20] Z. Johari and R. Ismail, Nanoscale Res. Lett. **8**, 479 (2013).

[21] S. H. R. Sena, J. M. Pereira Jr., G. A. Farias, F. M. Peeters, and R. N. Costa Filho, J. Phys.: Condens. Matter **24**, 375301 (2012).

[22] S. G. Stuij, P. H. Jacobse, V. Juričić, and C. M. Smith, Phys. Rev. B **92**, 075424 (2015).

[23] P. Y. Huang, C. S. Ruiz-vargas, A. M. Van Der Zande, W. S. Whitney, M. P. Levendorf, J. W. Kevek, S. Garg, J. S. Alden, C. J. Hustedt, Y. Zhu, J. Park, P. L. Mceuen, and D. A. Muller, Nature (London) **469**, 389 (2011).

[24] C. J. Páez, A. L. C. C. Pereira, J. N. B. B. Rodrigues, and N. M. R. R. Peres, Phys. Rev. B **92**, 045426 (2015).

[25] N. Levy, S. A. Burke, K. L. Meaker, M. Panlasigui, A. Zettl, F. Guinea, A. H. Castro Neto, and M. F. Crommie, Science **329**, 544 (2010).

[26] M. Schneider, D. Faria, S. Viola Kusminskiy, and N. Sandler, Phys. Rev. B **91**, 161407 (2015).

[27] T. Stegmann and N. Szpak, New J. Phys. **18**, 053016 (2016).

[28] P. Rodriguez-Lopez and A. Cortijo, Phys. Rev. B **97**, 235128 (2018).

[29] D. Zhai, K. Ingersent, S. E. Ulloa, and N. Sandler, Phys. Rev. B **99**, 195410 (2019).

[30] S. Babaee Touski and M. Pourfath, Appl. Phys. Lett. **103**, 143506 (2013).

[31] R. Carrillo-Bastos, D. Faria, A. Latgé, F. Mireles, and N. Sandler, Phys. Rev. B **90**, 041411 (2014).

[32] D. Moldovan, M. Ramezani Masir, and F. M. Peeters, Phys. Rev. B **88**, 035446 (2013).

[33] V. Torres, P. Silva, E. A. T. De Souza, L. A. Silva, and D. A. Bahamon, Phys. Rev. B **100**, 205411 (2019).

[34] D. A. Bahamon, Z. Qi, H. S. Park, V. M. Pereira, and D. K. Campbell, Nanoscale **7**, 15300 (2015).

[35] A. Georgi, P. Nemes-Incze, R. Carrillo-Bastos, D. Faria, S. Viola Kusminskiy, D. Zhai, M. Schneider, D. Subramaniam, T. Mashoff, N. M. Freitag, M. Liebmann, M. Pratzer, L. Wirtz, C. R. Woods, R. V. Gorbachev, Y. Cao, K. S. Novoselov, N. Sandler, and M. Morgenstern, Nano Lett. **17**, 2240 (2017).

[36] J. A. Lawlor, C. G. Rocha, V. Torres, A. Latgé, and M. S. Ferreira, J. Phys.: Condens. Matter **28**, 235001 (2016).

[37] D. Zhai and N. Sandler, Phys. Rev. B **98**, 165437 (2018).

[38] S. P. Milovanović and F. M. Peeters, J. Phys.: Condens. Matter **29**, 075601 (2017).

[39] V.-T. Tran, J. Saint-Martin, P. Dollfus, and S. Volz, AIP Adv. **7**, 075212 (2017).

[40] C. Si, Z. Sun, and F. Liu, Nanoscale **8**, 3207 (2016).

[41] G. Tahmasebipour, Y. Hojjat, V. Ahmadi, and A. Abdullah, Scanning **31**, 65 (2009).

[42] J. A. Morán Meza, C. Lubin, F. Thoyer, K. A. Villegas Rosales, A. A. Gutarra Espinoza, F. Martin, and J. Cousty, Carbon N. Y. **86**, 363 (2015).

[43] Y. Lu, Y. Chen, J. Xu, T. Wang, and J.-T. Lü, Opt. Express **26**, 30444 (2018).

[44] X. Li, X. Wang, L. Zhang, S. Lee, and H. Dai, Science **319**, 1229 (2008).

[45] R. M. Jacobberger, B. Kiraly, M. Fortin-Deschenes, P. L. Levesque, K. M. McElhinny, G. J. Brady, R. Rojas Delgado, S. Singha Roy, A. Mannix, M. G. Lagally, P. G. Evans, P. Desjardins, R. Martel, M. C. Hersam, N. P. Guisinger, and M. S. Arnold, Nat. Commun. **6**, 1 (2015).

[46] V. M. Pereira, A. H. Castro Neto, and N. M. R. Peres, Phys. Rev. B **80**, 045401 (2009).

[47] S. Datta, Superlattices Microstruct. **28**, 253 (2000).

[48] M. P. L. Sancho, J. M. L. Sancho, and J. Rubio, J. Phys. F: Met. Phys. **14**, 1205 (2000).

[49] C. H. Lewenkopf and E. R. Mucciolo, J. Comput. Electron. **12**, 203 (2013).

[50] V.-T. Tran, J. Saint-Martin, and P. Dollfus, Nanotechnology **26**, 495202 (2015).

[51] V. Torres, D. Faria, and A. Latgé, Phys. Rev. B **97**, 165429 (2018).

[52] C. P. P. Chang, Y. C. C. Huang, C. L. L. Lu, J. H. H. Ho, T. S. S. Li, and M. F. F. Lin, Carbon N. Y. **44**, 508 (2006).

[53] V.-T. T. Tran, J. Saint-Martin, and P. Dollfus, Appl. Phys. Lett. **105**, 073114 (2014).

[54] S. C. Chen, C. P. Chang, C. H. Lee, and M. F. Lin, J. Appl. Phys. **107**, 083712 (2010).

[55] C. Ritter, S. S. Makler, and A. Latgé, Phys. Rev. B **82**, 089903 (2010).

[56] T.-T. Vu and V. Tran, Semicond. Sci. Technol. **31**, 085002 (2016).

[57] S. Dorsch, B. Dalelkhan, S. Fahlvik, and A. M. Burke, Nanotechnology **30**, 144002 (2019).

[58] A. J. Du, Z. H. Zhu, Y. Chen, G. Q. Lu, and S. C. Smith, Chem. Phys. Lett. **469**, 183 (2009).

[59] A. Cresti, G. Grosso, and G. P. Parravicini, Phys. Rev. B **77**, 233402 (2008).

[60] J. Nakabayashi, D. Yamamoto, and S. Kurihara, Phys. Rev. Lett. **102**, 066803 (2009).